Nanostructure of the Epidermal Extracellular Space as Observed by Cryo-Electron Microscopy of Vitreous Sections of Human Skin

Ashraf Al-Amoudi,* Jacques Dubochet,† and Lars Norlén†‡

*Laboratory of Ultrastructural Analysis (LAU), Biology Building, University of Lausanne, Lausanne, Switzerland; †Department of Physics, University of Geneva, Geneva, Switzerland; ‡Department of Cellular and Molecular Biology (CMB), Karolinska Institute, Stockholm, Sweden

The newly developed method, cryo-electron microscopy of vitreous sections, was used to observe the nanostructure of the epidermal extracellular space. The data were obtained from vitreous sections of freshly taken, fully hydrated, non-cryo-protected human skin. The extracellular space of viable epidermis contains desmosomes, expressing a characteristic extracellular transverse ~5 nm periodicity, interconnected by a relatively electron lucent inter-desmosomal space. The extracellular space between viable and cornified epidermis contains transition desmosomes at different stages of reorganization interconnected by widened areas expressing a rich variety of complex membrane-like structures. The extracellular space of cornified epidermis contains ~9, ~14, ~25, ~33, ~39, ~44, and ~48 nm thick regions in turn containing one, two, four, six, eight, eight, and ten parallel electron-dense lines, respectively, between adjacent corneocyte lipid envelopes. The eight-line ~44 nm thick regions are most prevalent.

Key words: cadherin/CEMOVIS/ceramides/corneocytes/corneodesmosomes/cryo-electron microscopy/cryo-fixation/cryo-TEM/desmosomes/epidermis/skin barrier/skin lipids/stratum corneum/cubic membranes/cubic phases
J Invest Dermatol 124:764–777, 2005

Water homeostasis is a strict requirement for normal physiological function. The most important task of the human skin is thus to create a watertight enclosure of the body to prevent water loss. More precisely, it is the lipid-filled extracellular space of the cornified part of the epidermis (stratum corneum) that constitutes the main barrier toward transepidermal water loss (Blank, 1952).

An increased knowledge of the formation and molecular organization of the stratum corneum extracellular space may provide for a better understanding of skin diseases displaying impaired barrier function (e.g., atopic dermatitis) and suggest new approaches to optimize transdermal drug delivery and barrier restorative manipulations (e.g., skin protection, cosmetic formulations, etc.), respectively.

Desmosomes are major components of the extracellular space of viable epidermis. Even though the composition and biochemistry of desmosomes are fairly well characterized (Burdett, 1998; North *et al*, 1999), the finer molecular architecture *in situ* remains only partly defined both with respect to the extracellular core domain and the cytoplasmic plaque (He *et al*, 2003). Conventional electron microscopy on human skin has shown that ~40% of the length of the extracellular space of top-most viable epidermis (stratum granulosum) is occupied by desmosomes. The desmosome extracellular core domain shows a trilamellar optical density (OD) pattern that is modified into an electron-dense "plug" in the stratum corneum (Skerrow *et al*, 1989). Using ruthenium tetroxide staining, it has been shown that the stratum corneum (corneo)desmosome plug is composed of three dense lines separated by two clearer spaces (Haftek *et al*, 1998). Non-peripheral corneodesmosomes are gradually lost in the lower stratum corneum and absent above the fifth corneocyte layer (Chapman and Walsh, 1990).

The extracellular space between viable and cornified epidermis has been shown to express inter-desmosomal widenings containing bent multilamellar lipid sheets, and granular-like material (Fartasch *et al*, 1993; Norlén *et al*, 2003). Also, loosely arranged ondulating lamellae, separated by wide electron-lucent spaces and linked peripherally to the electron-dense corneodesmosome plug, have been reported to occupy the upper part of these regions (Menon *et al*, 1992; Fartasch *et al*, 1993).

Conventional electron microscopy has shown that the extracellular space of cornified epidermis expresses a multilamellar broad–narrow–broad electron lucent band pattern with an ~13 nm periodicity (Madison *et al*, 1987; Swartzendruber *et al*, 1989; Hou *et al*, 1991). Further, small-angle X-ray diffraction (SAXD) on the stratum corneum has shown 4.0–4.4, 5.8–6.6, and 12.9–13.6 nm reflections attributed to lamellar lipid conformations (Bouwstra *et al*, 1991; Garson *et al*, 1991; Hou *et al*, 1991; Schreiner *et al*, 2000; Ohta *et al*, 2003). Present models on the lamellar organization of the stratum corneum extracellular space are based on (a) ~13 nm repeats of a trilamellar "lipid bilayer/interdigitated half-thickness lipid bilayer/lipid bilayer" conformation (Bouwstra *et al*, 2000), (b) ~13 nm repeats of a triple "mixed lipid bilayer–monolayer" ~4.3 nm subunits conformation (Hill and Wertz, 2003), or (c) ~13 nm repeats of a bilamellar

Abbreviation: OD, optical density

"asymmetric lipid bilayer with a fluid space on one side of each lipid bilayer" conformation (McIntosh, 2003).

Water is the major constituent of cells. But much of our knowledge of skin ultrastructure has been gained from observations on dry, chemically fixed, stained, and plastic-embedded specimens. It is possible, therefore, that the deleterious effects of conventional specimen preparation for electron microscopy may not have been fully acknowledged in the present perception of epidermal structural organization. This may be particularly true for liquid crystalline and/or paracrystalline entities such as biological lipid structures as water activity represents a major factor determining lipid phase behavior and structural organization (Guldbrand *et al*, 1982; Small, 1986; Israelachvili, 1992; Evans and Wennerström, 1994, pp. 440–443; Larsson, 1994). The effect of dehydration on the extracellular lipid matrix of the lowly hydrated stratum corneum may, however, be considerably smaller than on more highly hydrated lipid structures of viable epidermal cell layers.

During the last two decades, cryo-electron microscopy has been increasingly used in order to observe biological samples in their fully hydrated state (Dubochet *et al*, 1988). Typically, the method consists in vitrifying (which means that cooling is so rapid that ice-crystals do not have time to form) a thin film of a suspension of macromolecules and observing it in a cryo-electron microscope at a temperature where vitreous water is stable and does not evaporate ($<-140^{\circ}$C). The native structure of the specimen may then be preserved down to atomic resolution. Further, biostructures are often better visualized unstained in their aqueous environment than stained in conventional preparations. This is because the signal-to-noise ratio is optimal in vitreous water, where the major source of noise comes from the statistics of electron scattering.

Recently, the method has been extended to specimens that are too large to be squeezed into a thin liquid film (Norlén *et al*, 2003; Al-Amoudi *et al*, 2004; Norlén and Al-Amoudi, 2004). This requires successful vitrification of bulky specimens and that ultra-thin cryo-sections subsequently can be cut and observed. Although cryo-electron microscopy of vitreous sections (CEMOVIS) probably provides a more faithful representation of cells and tissues than any previous electron microscopy method, artifacts because of high-pressure freezing, cutting deformation, and electron beam damage must still be considered.

Tissue CEMOVIS was used to study the human epidermis as one of its first practical applications (Norlén *et al*, 2003). In this recent work, the image resolution was limited by a comparatively large cryo-section thickness ($\sim$100 nm) and mediocre section quality, which in turn prevented a more detailed structural analysis. Since then, we have been able to improve the quality of the cryo-sections (i.e., reduced section thicknesses and cutting artifacts) and imaging conditions (i.e., optimal magnification focus and electron dose). As a result, the morphology of the epidermal extracellular space is revealed with more detail (nanometer range). A number of complex multilamellar architectures of the stratum corneum extracellular space are identified and several intermediate stages of their formation process, involving coordinated desmosome and lipid membrane transformations, are demonstrated.

Results

Methodological evaluation Optimization of the sample preparation technique, notably a more homogenous sample size and sample thickness, yielded a complete full-thickness vitrification of human forearm epidermis with an approximately 80% success rate. The highly hydrated underlying dermis was vitrified with an approximately 20% success rate. The diffraction patterns of vitrified frozen hydrated human mid-volar forearm epidermis showed a first diffuse ring corresponding to 0.36 nm, typical of high-density vitreous water (cf. Dubochet *et al*, 1988, p. 143).

Optimization of the cryo-sectioning technique decreased the median thickness of the cryo-sections to $\sim$ 50 nm (range 30–80 nm, number of sections examined = 20). This in turn allowed for high-resolution images to be obtained. On the $\sim$ 50 nm thick sections, an instrumental resolution better than 2 nm was regularly achieved as judged from the extension of the transfer function. Compression along the cutting direction was in the order of 30%–50%. Knife marks and chatter were present on many vitreous sections of cryo-fixed epidermis, but did not significantly affect the information content of the micrographs.

Ultrastructural evaluation

The extracellular space of viable epidermis Figures 1 (*lower part*) and 2 show typical views of the extracellular space of viable epidermis at low and high magnification, respectively. Conventional desmosomes were exclusively found in the viable part of the epidermis (Fig 1, *open white arrows*). They were interconnected by highly folded regions of the extracellular space (Fig 2*A*, *black asterisk*) showing no apparent internal fine structure.

The desmosome fine structure (Fig 2*A*, *B*) appeared identical throughout the viable epidermis. The desmosome extracellular core domain had a median thickness of 32.6 nm (27.9–38.7 nm, n = 12) and expressed a characteristic transverse 5.3 nm (4.5–6.9 nm, n = 13) periodicity (Fig 2*B*, *solid black arrow*). The desmosome plasmamembranes (Fig 2*B*, *open white arrow*) appeared as 4.0 nm (3.7–4.3 nm, n = 12) thick (measured as the center-to-center distance between the two opposed electron-dense lines) high-density double-layer patterns. On their cytoplasmic side, a 12.7 nm (10.8–15.1 nm, n = 12) thick zone of medium electron density (*white asterisks*) separated the electron-dense plasmamembrane from two parallel electron-dense layers, situated 6.7 nm (4.9–7.4 nm, n = 12) apart and interconnected by traversing electron-dense lines with a 6.6 nm (4.8–8.1 nm, n = 8) periodicity (Fig 2*B*, *solid white arrow*). This $\sim$ 6.7 nm thick double layer was in turn paralleled on each side by a very weak electron-dense line (Fig 2*A*, *thin white arrows*).

The extracellular space between viable and cornified epidermis The extracellular space between viable and cornified epidermis was characterized by a rich variety of complex features. About half of the length of the extracellular space was occupied by structures reminiscent of desmosomes but differing in many respects (hereafter referred to as "transition desmosomes") (Fig 1, *solid white arrows*). The remaining half was occupied by widened areas, frequently extending as deep cell invaginations (Fig 1, *thin*

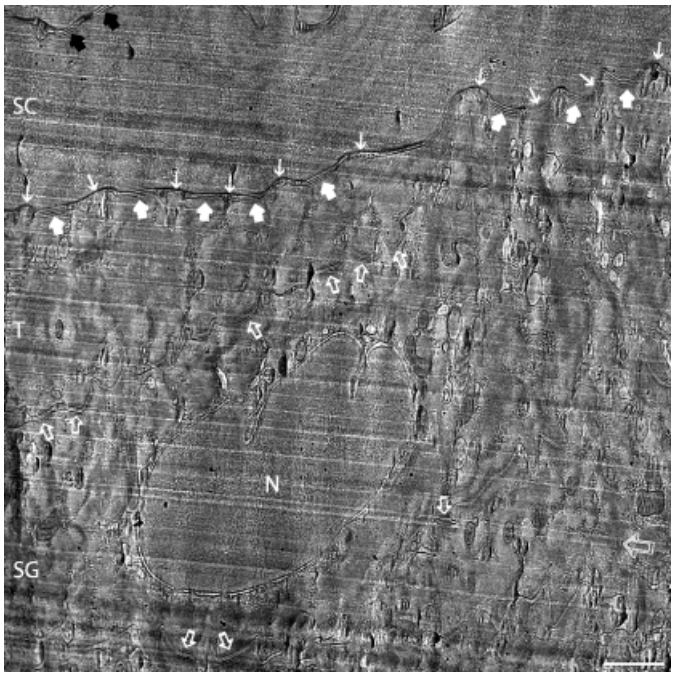

Figure 1
Transition desmosomes are exclusively found at the interface between stratum granulosum and stratum corneum. Low-magnification cryo-transmission electron micrograph of vitreous section of human epidermis at the interface between viable and cornified cell layers. About 50% of the extracellular space at this location is occupied by transition desmosomes (*solid white arrows*) and the remaining 50% by widened areas (*thin white arrows*) containing complex electron density patterns (cf. Figs 3 and 4). *Open white arrows*: desmosomes (cf. Fig 2); *Solid black arrows*: ~ 44 nm thick regions of the stratum corneum extracellular space (cf. Fig 8). N, nucleus; SG, uppermost stratum granulosum cell; T, transition cell; SC, lowermost stratum corneum cell. *Open white double arrow*: section cutting direction. Section thickness ~ 50 nm. *Scale bar*, 500 nm.

white arrows), containing complex membrane-like structures.

The most frequently observed internal feature of widened areas was a stacked (usually bent) multilamellar electron density pattern (n = 19) associated with a granular pattern (n = 25) (Fig 3*A*; *white asterisks* in Fig 4*A*, *C*). Other patterns observed were as follows: (a) Check patterns (n = 5) (Fig 3*A*, *central white box*) incorporated in a complex arrangement of irregular layers; (b) Multilamellar electron densities enclosing a granular structure (n = 1) (Fig 3*B*). The region visualized in Fig 3*B* is probably a cross-section through a large invagination originating at the interface between viable and cornified epidermis (*inset box*, *solid white arrows*). The multilamellar "shell" domain was composed of at least 25 electron-dense lines at its thickest part, with an apparent decreasing lamellar repeat distance from ~ 5 nm in the central part to ~ 4 nm in the peripheral part; (c) Complex stacks of small portions of bent double-layer electron density patterns (n = 4) (Fig 4*B*, *white box*); (d) stacks of electron-dense double-layer patterns (Fig 4*D*, *region "1"*) seemingly extending into the extracellular core domain of transition desmosomes (n = 7) (Fig 4*A*, *open white arrow*).

No widened extracellular areas were found above the third stratum corneum cell, although apparently featureless extracellular dilatations were observed throughout the mature stratum corneum (cf. Fig 5*A*, *C*, *black asterisks*). In the first to third stratum corneum extracellular space loosely packed extended double-layer patterns (n = 14) (pairs of thin white arrows) were found in remaining widened areas (Fig 6*A*). The most peripheral double-layer patterns (peripheral-most pairs of thin white arrows) adhered closely to the corneocyte lipid envelope (pair of thin black arrows) giving the corneocyte cell periphery a trilamellar aspect (n = 5) (Fig 6*A*, *B*, *small square bracket*). The loosely packed extended double-layer patterns were observed to be associated laterally either with the characteristic eight-line pattern of ~ 44 nm thick regions (Fig 6*B*, *C*, large, square bracket) or with the stacked lamellae of linker regions (Fig 7*A*, *C*, *large white box*).

Transition desmosomes were recognized at low magnification by the fact that they lacked a cytoplasmic plaque on the upper (corneocyte) side (Fig 1, *solid white arrows*). In contrast to normal desmosomes (*open white arrows*) they therefore appeared asymmetric. Transition desmosomes were exclusively found at the interface between the stratum granulosum and stratum corneum. High-magnification views are shown in Fig 4. The median width of the extracellular core domain of transition desmosomes was 43.4 nm (38.5–47.9 nm, n = 29) (Table I). The single cytoplasmic plaque on the lower (stratum granulosum) side was characterized by a central ~ 10 nm thick electron-dense band (Fig 4*A–D*, *solid white arrows*), paralleled on each side by a very weak ~ 2–4 nm thick electron-dense double line (Fig 4*C*, *thin white arrow in inset box*; *B*, *D*, *thin black arrows*). The cytoplasmic plaque was situated ~ 11 nm from the plasmamembrane of the uppermost stratum granulosum cell. The transition desmosome single cornified envelope was characterized by an intracellular ~ 16–18 nm thick diffuse electron-dense band situated adjacent to two electron-dense lines representing the corneocyte lipid envelope (Fig 4*A–D*, *solid black arrows*). The transition desmosome extracellular core domain contained a combination of (a) a multilamellar electron density pattern (n = 22) (Fig 4*C*, *inset box*; *D*, *region "3"*) of which a central electron-dense double-layer pattern was most prominent (Fig 4*C*, inset box; *D*, *open white arrow*), (b) a granular electron density pattern (n = 7) (Fig 4*D*, *region "2"*), and (c) a stack of four (in most cases) and up to six paired electron-dense lines (n = 7) (Fig 4*A*, *open white arrow*; cf. also Fig 4*D*, *region "1"*).

The detailed extracellular multilamellar electron density pattern of transition desmosomes (Fig 4*C*, *inset box*) was characterized by a central electron-dense double-layer pattern paralleled on each side by three weaker electron-dense lines (*thin black arrows*). The outermost (as measured from the central electron-dense double layer) weak line ran adjacent to the outer electron-dense line of the two electron-dense lines forming either the corneocyte lipid envelope (*upper side*) or the stratum granulosum cell plasmamembrane (*lower side*). The plasmamembrane/lipid envelope line spacing (i.e., width) was 4.4 nm (4.0–4.8 nm, n = 22) and the line spacing of the two electron-dense lines forming the central electron-dense double-layer pattern was 4.9 nm (4.0–6.3 nm, n = 22). The first (peripheral-most) line of the transition desmosome extracellular space was situated at a distance of 4.7 nm (range 4.2–5.6 nm, n = 22) from the outer electron-dense line of the double-layer pattern forming the corneocyte lipid envelope (*upper side*) or plasmamembrane

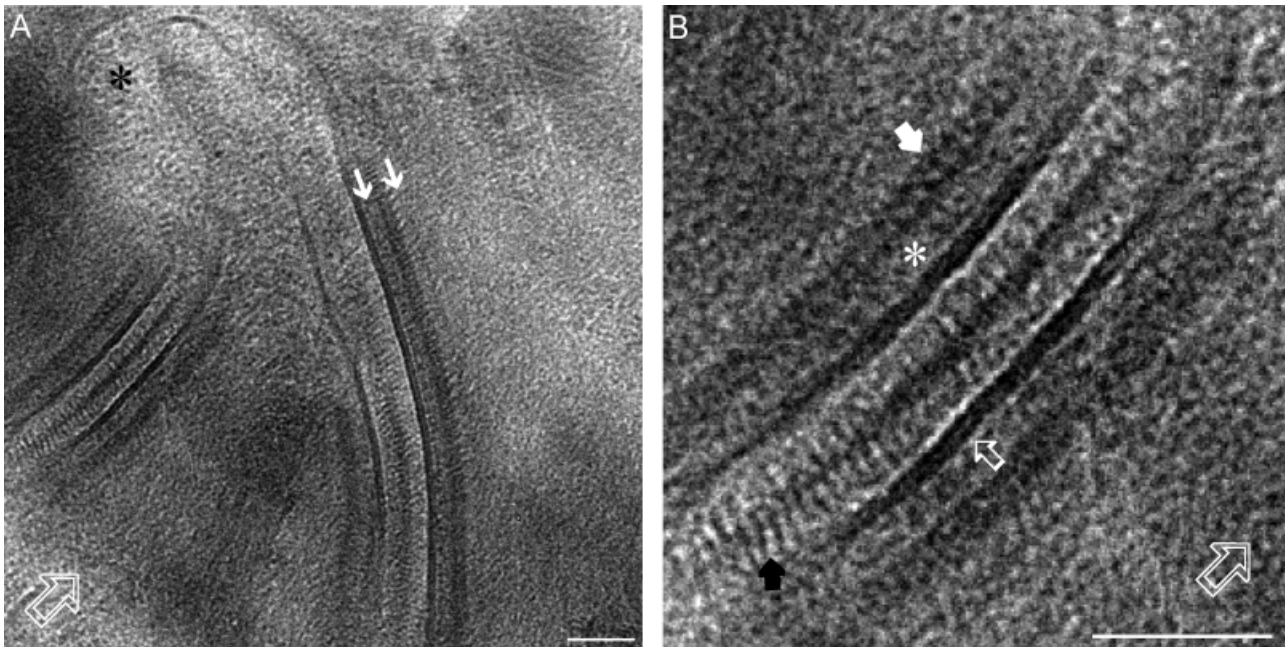

Figure 2
The desmosome extracellular core domain is characterized by an electron-dense transverse ~ 5 nm periodicity. High-magnification cryo-electron micrograph of desmosomes at the midportion of the viable part of the human epidermis. (*B*) Represents an enlargement of the middle left part of (*A*). The plasma membranes appear as ~ 4 nm thick high-density double-layer patterns (*B*, *open white arrow*). The extracellular core domain is ~ 33 nm thick (cf. Table I) and contains transverse electron-dense lines with an ~ 5 nm periodicity (*B*, *solid black arrow*), most probably corresponding to extracellular adhesion proteins (i.e., cadherins). On the cytoplasmic side, an ~ 11 nm thick zone of medium electron density (*B*, *white asterisk*) separates the electron-dense plasma membrane from two parallel electron-dense layers, situated ~ 7 nm apart and interconnected by traversing electron-dense lines with an ~ 6 nm periodicity (*B*, *solid white arrow*). The inter-desmosomal space (*black asterisk*) showed no apparent internal fine structure. *Thin white arrows* (*A*): very weak electron-dense lines associated with the desmosome cytoplasmic plaque; *open white double arrows* (*A*, *B*): section cutting direction. Section thickness ~ 50 nm. *Scale bar*: (*A*, *B*), 50 nm.

(*lower side*). The second line of the transition desmosome extracellular space was situated at a distance of 6.3 nm (4.6–8.0 nm, n = 22) from the first line and at a distance of 4.3 nm (range 3.2–5.7 nm, n = 22) from the third line. The third line was situated at a distance of 4.3 nm (range 3.7–4.9 nm, n = 22) from the adjacent line of the central electron-dense double-layer pattern (i.e., the fourth (strong) line of the transition-desmosome extracellular space) (Fig 4*C*, *inset box*). The extracellular space of transition desmosomes thus contained eight electron-dense lines with line spacings of approximately 4.5, 6.5, 4.5, 4.5, 5, 4.5, 4.5, 6.5, 4.5 nm between the corneocyte lipid envelope (*upper side*) and the plasmamembrane (*lower side*) (Fig 4*C*, *inset box*). The total thickness of the extracellular space varied between 39 and 48 nm (Table I).

The extracellular space of cornified epidermis High-magnification views of extracellular space of cornified epidermis are shown in Figs 8–10. At low magnification, the extracellular space of fully differentiated stratum corneum (i.e., above the third cell layer) showed a seemingly identical morphology throughout the tissue (with the possible exception of the outermost desquamating cell layers that were not studied) (Fig 5*A*). It was dominated by ~ 44 nm thick regions (cf. Fig 5*B*, *C*, *open black arrows*; Fig 8; Table I) interconnected by thinner linker regions (Fig 5*C*, *D*, *solid black arrows*; Figs 9*A*–*H*; Table I). The ~ 44 nm thick regions occupied the major portion of the extracellular space of both lower (Fig 5*B*, *open black arrows*) and mid-part (Fig 5*C*, *open black arrows*) stratum corneum, often extending laterally over more than 1 μm (Fig 5*C*, *open black arrows*). The measures of lateral extension may, however, be regarded with some reservation as close to perpendicular orientation of the extracellular space in the section was difficult to obtain over longer (μm) distances because of the undulated nature of the corneocyte surface. Linker regions were usually short (Fig 5*C*, *D*, *solid black arrows*), but could extend laterally over more than 250 nm (Fig 9*A*, *C*). Apparent dilatations of the extracellular space were observed in many sections (Fig 5*A*, *C*, *black asterisks*), both in lower and in mid-part stratum corneum. At high magnification, no internal structure was observed (not shown).

The ~ 44 nm thick regions contained eight electron-dense parallel lines with a characteristic pattern: a central electron-dense double-layer pattern paralleled on each side by three weaker electron-dense lines (Fig 8, *inset box A*). The mid-line of the three weaker electron-dense lines was stronger than the two lines surrounding it. The outermost (as measured from the central electron-dense double-layer pattern) weak line ran adjacent to the outer electron-dense line of the two electron-dense lines forming the corneocyte lipid envelope (which in turn separated the extracellular space from the diffuse electron-dense cornified envelope). All line spacings are shown in Fig 8 (*inset box A*). The line spacing of the two electron-dense lines forming the corneocyte lipid envelope was 4.4 nm (3.8–5.0 nm, n = 13) and the line spacing of the two electron-dense lines forming the central double-layer pattern was 4.3 nm (4.1–4.6 nm, n = 13). The first (weak) line of the extracellular space was situated at a distance of 4.4 nm (3.6–5.2 nm, n = 13) from

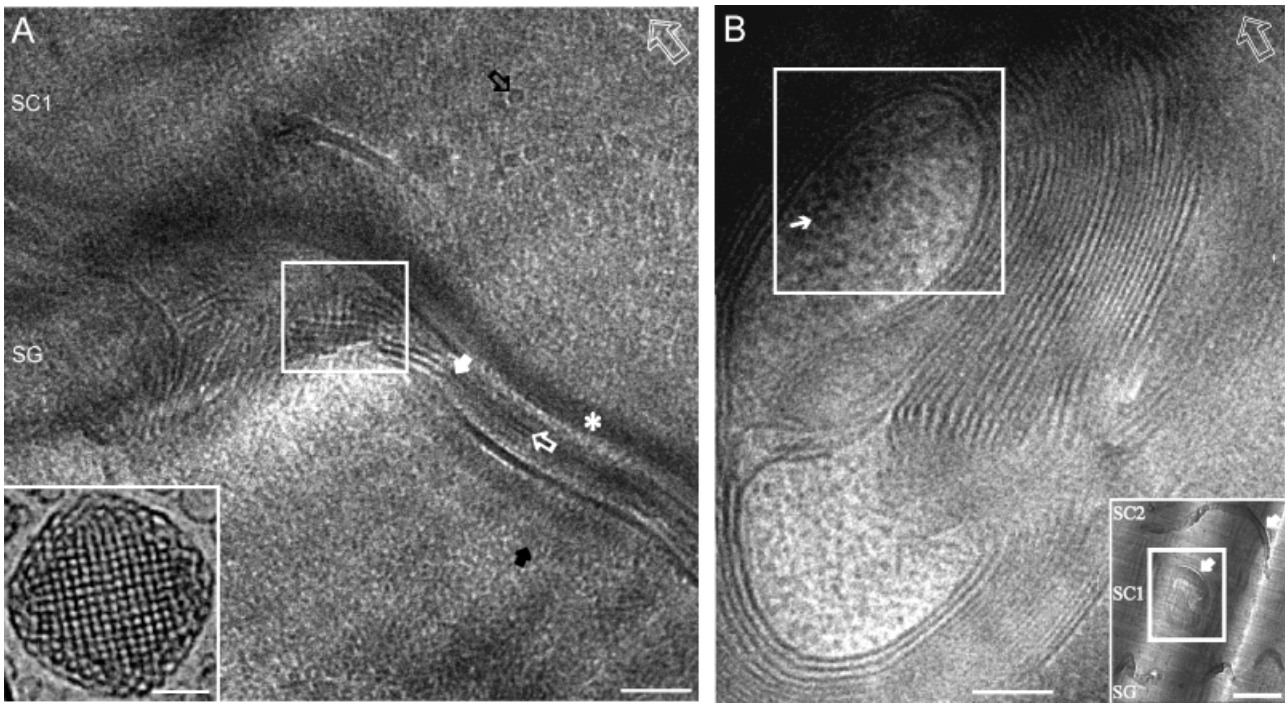

Figure 3
Check pattern (*A*) and bent multilamellar (*B*) electron density pattern in widened areas. High-magnification cryo-electron micrographs (*A*, *B*) of widened areas of the extracellular space between stratum granulosum and stratum corneum of vitreous epidermis. The electron density check pattern in (*A*) (*central white box*) resembles, including its dimensions, the cryo-electron density pattern of cubic lipid/water *in vitro* phases (*A*, *inset box*). *Open white arrow* (*A*): central electron-dense double-layer pattern of transition-desmosome extracellular core domain in possible continuity (*solid white arrow*) with lamellar lipid material of adjacent widened areas (*A*, *central white box*); *solid black arrow* (*A*): remnants of the inner cytoplasmic desmosome plaque; SG (*A*): uppermost stratum granulosum cell; SC1 (*A*): lowermost stratum corneum cell; white asterisk (*A*): cornified envelope; open black arrow (*A*): keratin intermediate filament cut perpendicularly to its length axis; thin white arrow (*B*): sinusoid-like dot-pattern. Inset box (*A*): cryo-transmission electron micrograph of a lipid/water *in vitro* phase with cubic (D-type) symmetry (*scale bar*, 50 nm), from Spicer *et al* (2001), with permission from the ACS Publications. *Inset box* (*B*): low-magnification cryo-electron micrograph of the locality from which (*B*) was obtained (*white box*). *Solid white arrows* (*B*, *inset box*): extracellular space; *open white double arrow* (*A*, *B*): section cutting direction. Section thickness (*A*, *B*) $\sim$ 50 nm. *Scale bar*: (*A*, *B*), 50 nm; (*B*, *inset box*), 500 nm.

the outer electron-dense line of the double-layer pattern forming the corneocyte lipid envelope. The second (medium electron dense) line of the stratum corneum extracellular space was situated at a median distance of 6.3 nm (5.5–7.1 nm, n = 13) from the first (weak) line and at a median distance of 4.3 nm (3.8–4.7 nm, n = 13) from the third (weak) line. The third (weak) line was situated at a median distance of 4.2 nm (3.8–4.6 nm, n = 13) from the adjacent line of the central electron-dense double-layer pattern (i.e., the fourth (strong) line of the extracellular space). The eight-line pattern of the $\sim$ 44 nm thick regions of the stratum corneum extracellular space thus closely resembled the eight-line pattern of the extracellular space of transition desmosomes (cf. Fig 4*C*, *inset box*). In some stratum corneum eight-line regions, the total thickness of the extracellular space was smaller (38.7–40.0 nm, n = 5; Table I) than $\sim$ 44 nm and the line spacings slightly different from the characteristic pattern (cf. Fig 6*C*, *white square bracket*). Further, a minority of regions showed a ten-line pattern with a thickness of the intercellular space of 48.3 nm (47.9–49.3 nm, n = 3) (Fig 8, *inset box B*) (Table I) in which four (and not three as in the $\sim$ 44 nm thick regions) approximately equally spaced electron-dense lines were visible on each side of the central electron-dense double layer (*thin white arrows*).

Four different types of linker regions were observed, with a median thickness of the extracellular space of 9.0 nm (8.2–11.6 nm, n = 5), 14.1 nm (13.6–14.9 nm, n = 3), 25.3 nm (23.7–28.9 nm, n = 3), and 33.1 nm (30.8–36.4 nm, n = 3), respectively (Table I). The $\sim$ 9 nm thick linker regions contained one electron-dense line (Fig 9*E–G*, *thin white arrows*), the $\sim$ 14 nm thick linker regions' two lines contained (Fig 9*A*, *B*, *thin white arrows*), the $\sim$ 25 nm thick linker regions' contained four lines (Fig 9*C*, *D*, *thin white arrows*), and the $\sim$ 33 nm thick linker regions' contained six lines (Figs 9*H*, *thin black arrows*; 7*C*, *thin white arrows*) with an approximately uniform line spacing of 4–5 nm. In addition to the smaller thickness of the extracellular space, the four- and six-line linker regions differed most typically from the dominating $\sim$ 44 nm thick eight-line regions in that all their lines were of approximately uniform electron density.

In order to complete the picture, Fig 10 shows some additional structures observed in rare cases. One micrograph from the lower mid-part stratum corneum extracellular space showed a desmosome-like structure with a periodic cytoplasmic plaque electron density pattern (Fig 10*A*, *solid white arrows*). Neither an extracellular transverse $\sim$ 5 nm periodicity, nor a multilamellar electron density pattern, or signs of a cornified envelope, were visible. The width of the extracellular domain was $\sim$ 34 nm (Table I). Furthermore, the plasmamembrane-like double-layer pattern was more electron dense than the corneocyte lipid envelope double-layer pattern of the $\sim$ 44 nm thick regions (cf. Fig 8).

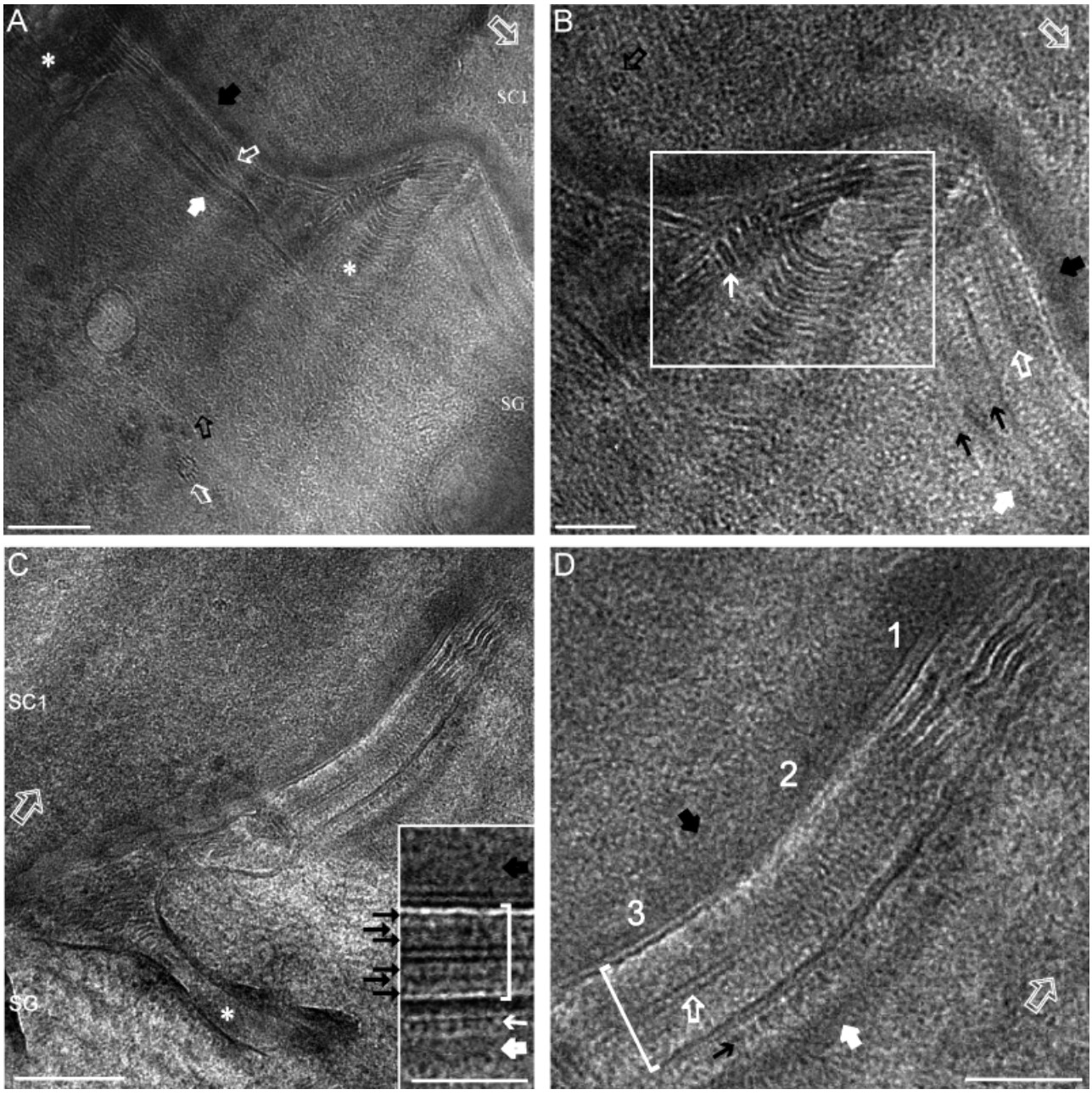

Figure 4
Transition desmosomes. High-magnification cryo-electron micrographs of the interface between stratum granulosum and stratum corneum of vitreous epidermis (*B*, *D* represent enlargements of the upper right part of *A*, *C*, respectively). Transition desmosomes are characterized by an ~ 43 nm thick extracellular core domain *white square brackets* in (*D*, and *C*, *inset box*; Table I) and by a single cornified envelope (*solid black arrows*) situated on the upper cytoplasmic side and a single cytoplasmic plaque (*solid white arrows*) situated on the lower cytoplasmic side. Note that a stacked lipid bilayer-like material (*D*, *region "1"*) sometimes appears in the transition-desmosome extracellular core domain (*A*, *open white arrow*) already before the desmosome cytoplasmic plaque (*A*, *solid white arrow*) has disappeared. Widened areas (*A*, *C*, *white asterisks*) between transition desmosomes express a complex electron density pattern (*B*, *white box*; cf. Fig 3). The flattened circular electron-dense structure marked by a thin white arrow inside the white box in (*B*) has a thickness of ~ 3.9 nm, excluding an underlying flattened vesicular (i.e., lamellar body disc) morphology. *Solid white arrows* (*A–D*): transition-desmosome cytoplasmic plaque; *solid black arrows* (*A–D*): cornified envelope; *thin black arrows* (*B*, *D*): very weak electron-dense lines associated with the transition-desmosome cytoplasmic plaque (*C*, *thin white arrow in inset box*); *open white arrows* (*B*, *D*): electron-dense central double-layer pattern of the transition-desmosome extracellular domain; *white asterisks* (*A*, *C*): widened areas; SG: uppermost stratum granulosum cell; SC1: lowermost stratum corneum cell; *open black arrows*: keratin intermediate filaments in keratinocyte (*A*) and corneocyte (*B*) cut approximately perpendicular to their length axis; *oblique open white arrow* (*A*): microtubule; *open white double arrows* (*A–D*): section cutting direction. Section thickness (*A–D*), ~ 50 nm. *Scale bars*: (*A*, *C*), 100 nm; (*B*, *D*; *C*, *inset box*), 50 nm.

The structure shown in Fig 10*B* is reminiscent of the ~ 44 nm thick regions (cf. Fig 8) except for the fact that it presents an extended cornified envelope and signs of cytoplasmic plaques (*solid black arrows*).

Discussion

Here we present detailed cryo-electron microscopy observations on the native structural organization of the

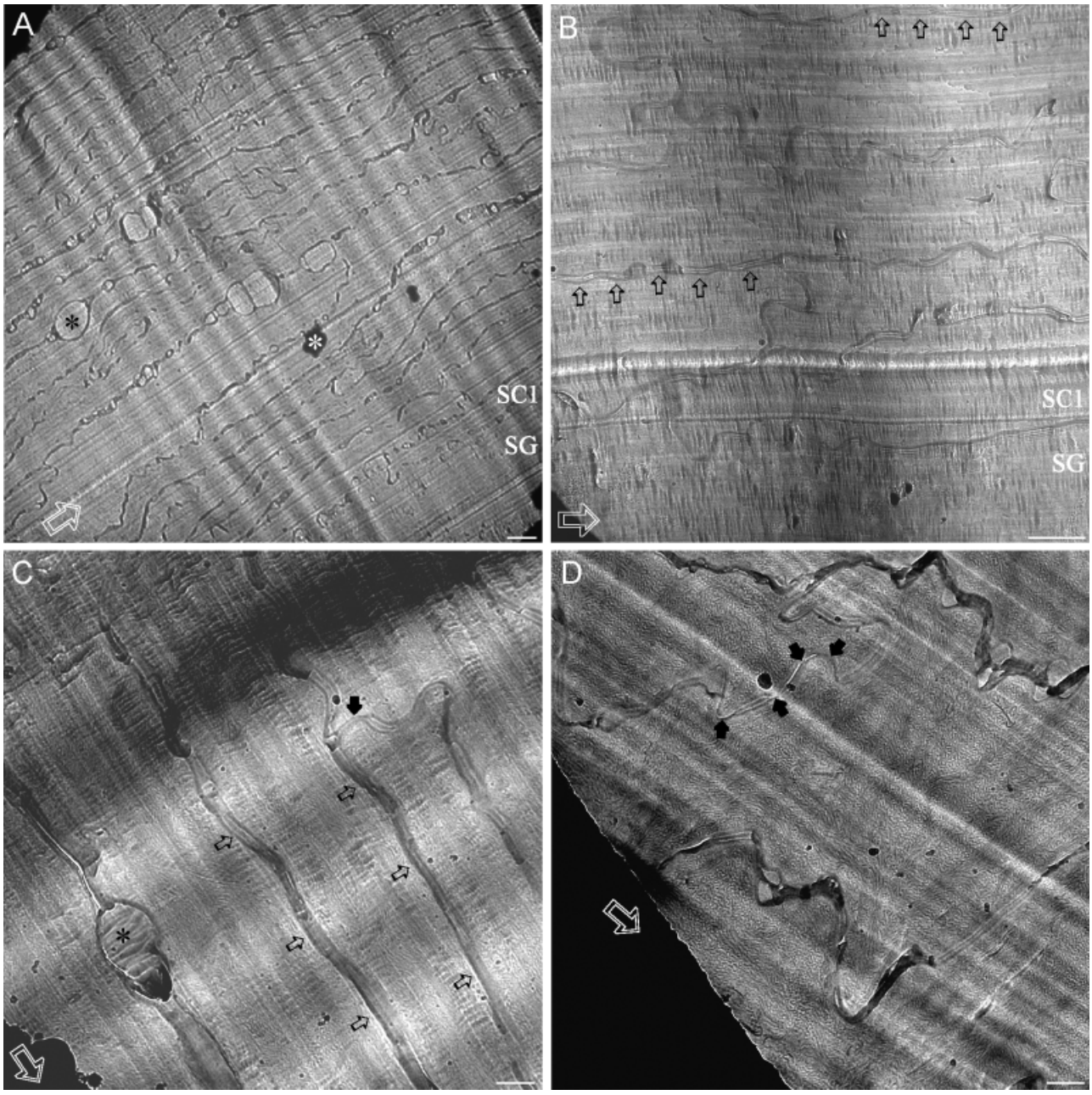

Figure 5
The stratum corneum extracellular space is dominated by ~ 44 nm thick regions, interconnected by thinner linker regions. (*A–D*) Low-magnification cryo-electron micrographs of stratum corneum of vitreous sections. (*A*) Overview of stratum corneum. (*B*) Lower stratum corneum. (*C*, *D*) Mid-portion of stratum corneum. The extracellular ~ 44 nm thick regions (*B*, *open black arrows*) may extend over > 1 μm (*C*, *open black arrows*) and are interconnected by thinner linker regions (*C*, *D*, *solid black arrows*). At the cell edges (*D*), these linker regions may extend over distances of > 250 nm (cf. Fig 9*A*). *Black asterisks* (*A*, *C*): apparent dilatations of the extracellular space; *white asterisk* (*A*): surface ice contamination; SG: uppermost stratum granulosum cell; SC1: lowermost stratum corneum cell; *open white double arrows* (*A–D*): section cutting direction. Section thickness (*A–D*) ~ 50 nm. *Scale bars*: (*A*, *B*), 500 nm; (*C*, *D*), 200 nm.

epidermal extracellular space and how it is transformed during differentiation. Starting from a structurally relatively simple and stable initial state, represented by the extracellular space of a viable epidermis, a sudden transformation takes place at the interzone between viable and cornified epidermis. This transformation gives rise to another relatively simple and stable final state, represented by the extracellular space of cornified epidermis. The initial state corresponds to viable desmosomes interconnected by a relatively electron lucent interspace. The final state corresponds to eight- and ten-line patterns interconnected by one-, two-, four-, and six-line patterns. In the extracellular space between the viable and cornified epidermis, we observe a wealth of structures comprising modified desmosomes interconnected by complex membrane-like morphologies.

Initial state: The extracellular space of viable epidermis The desmosomal fine structure appeared identical throughout the viable epidermis, whereas the extracellular

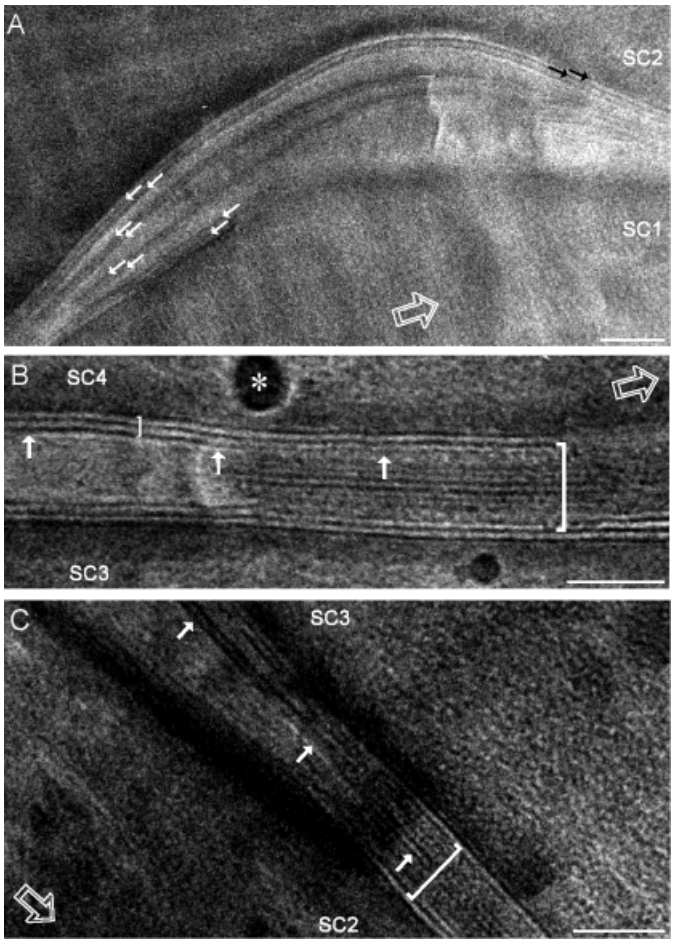

Figure 6
Loosely packed extended lipid bilayer-like structures are found in remaining widened areas of the lower stratum corneum. High-magnification cryo-transmission electron micrographs of lower stratum corneum of vitreous epidermis (*A–C*). The most peripheral double-layer patterns of remaining widened areas (*A*, *pairs of thin white arrows*) adhere closely to the corneocyte lipid envelope (*A*, *pairs of thin black arrows*). This is expressed as a characteristic trilamellar electron density pattern (*B*, *small white square bracket*) that seems to be continuous (*B*, *thin white arrows*) with the peripheral lines of adjacent eight-line $\sim$ 44 nm thick regions (*B*, *large white square bracket*). More central double-layer patterns of remaining widened areas seem continuous (*C*, *thin white arrows*) with central lines of adjacent eight-line regions (*C*, *white square bracket*). SC1-4 (*A–C*) first to fourth stratum corneum cell; *open white double arrow* (*A–C*): section cutting direction. Section thickness (*A–C*) $\sim$ 50 nm. *Scale bar*: (*A–C*), 50 nm.

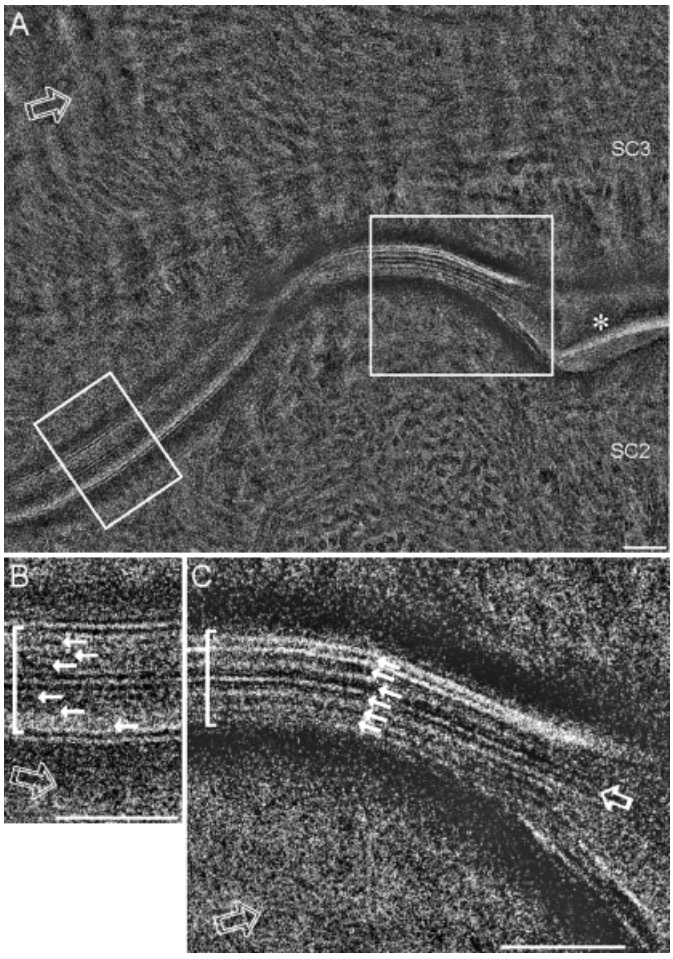

Figure 7
Loosely packed lipid bilayer-like structures are associated laterally to linker-regions in addition to $\sim$ 44 nm thick regions. High-magnification cryo-transmission electron micrograph of lower stratum corneum of vitreous epidermis (*A*). (*B*) Represents a magnification of the area marked by the small, left white box in (*A*). (*C*) Represents a magnification of the area marked by the large, right white box in (*A*). The loosely packed lipid bilayer-like patterns of a remaining widened area (*A*, *white asterisks*) seem to be in possible continuity (*C*, *open white arrow*) with parts of the six-line pattern (*C*, *thin white arrows*) of an $\sim$ 33 nm thick linker region (*C*, *white square bracket*). An $\sim$ 44 nm thick (*B*, *white square bracket*) eight-line (*B*, *thin white arrows*) region is seen adjacent to the six line $\sim$ 33 nm thick linker region in (*A*). SC2-3 (*A*): second and third stratum corneum cell; *open white double arrows* (*A–C*): section cutting direction. Section thickness $\sim$ 50 nm. *Scale bar*: (*A–C*), 50 nm.

inter-desmosomal space did not reveal any internal structure and did not show any signs of membranes or other features suggesting lipid morphologies (Fig 2*A*, *black asterisk*). At high magnification, the desmosome extracellular core domain expressed a characteristic $\sim$ 5 nm periodicity, most probably corresponding to cadherin adhesion molecules (Fig 2*B*, *solid black arrow*). Computerized electron tomography on freeze-substituted (i.e., dehydrated) neonatal mouse skin sections has recently shown desmosome cadherin molecules to be bent and irregularly spaced (He *et al*, 2003). Here we show, however, that in vitreous sections of fully hydrated human epidermis desmosome cadherin molecules are straight and regularly spaced (Fig 2). This discrepancy probably corresponds to a loss of structural order induced by dehydration during freeze substitution.

Final state: The extracellular space of cornified epidermis The stratum corneum extracellular space is dominated by $\sim$ 39, $\sim$ 44, and $\sim$ 48 nm thick regions interconnected by shorter $\sim$ 9, $\sim$ 14, $\sim$ 25, and $\sim$ 33 nm thick linker regions. The $\sim$ 44 nm thick regions express a characteristic band pattern with two central strong electron-dense lines paralleled on each side by three weaker electron-dense lines of which the central line usually is stronger than the two lines surrounding it (Fig 8, *inset box A*). The $\sim$ 9, $\sim$ 14, $\sim$ 25, and $\sim$ 33 nm thick linker regions and the $\sim$ 39 and $\sim$ 48 nm thick regions contain one, two, four, six, eight, and ten parallel electron-dense lines, respectively, with an approximately uniform line spacing of 4–5 nm. Except for the difference in the number of parallel lines present in the extracellular space, the $\sim$ 39 and $\sim$ 48 nm thick regions

Table I Structures of the epidermal extracellular space

Description	Extracellular space thickness (median, nm)	Range (nm)	Electron-dense central double-layer thickness (median, nm)	Range (nm)	Number of electron-dense lines in the extracellular space
Viable desmosomes	32.6	27.9–38.7 (n = 12)	—	—	—
Transition desmosomes	43.4	38.5–47.9 (n = 29)	4.9	4.0–6.3 (n = 22)	8
~ 9 nm thick regions	9.0	8.2–11.6 (n = 5)	—	—	1
~ 14 nm thick regions	14.1	13.6–14.9 (n = 3)	4.3	3.9–4.5 (n = 5)	2
~ 25 nm thick regions	25.3	23.7–28.9 (n = 3)	4.3	4.0–4.5 (n = 3)	4
~ 33 nm thick regions	33.1	30.8–36.4 (n = 3)	4.3	3.9–4.4 (n = 3)	6
~ 39 nm thick regions	39.0	38.7–40.0 (n = 5)	4.3	3.9–4.7 (n = 5)	8
~ 44 nm thick regions	43.6	41.7–46.0 (n = 28)	4.3	4.1–4.6 (n = 13)	8
~ 48 nm thick regions	48.3	47.9–49.3 (n = 3)	4.4	4.0–4.7 (n = 3)	10
~ 44 nm thick region with cytoplasmic plaques	42.9	41.3–44.1 (n = 1)	4.2	3.5–4.6 (n = 1)	8
"Corneodesmosome"	34.3	33.3–35.1 (n = 1)	—	—	—

differ most typically from the ~14, ~25, and ~33 nm thick linker regions in that their two central lines are more electron dense than the rest (Fig 6*C*, *white square bracket*; Fig 8, *inset box B*). This is not the case for linker regions, which express parallel lines with an approximately uniform electron density (Fig 9).

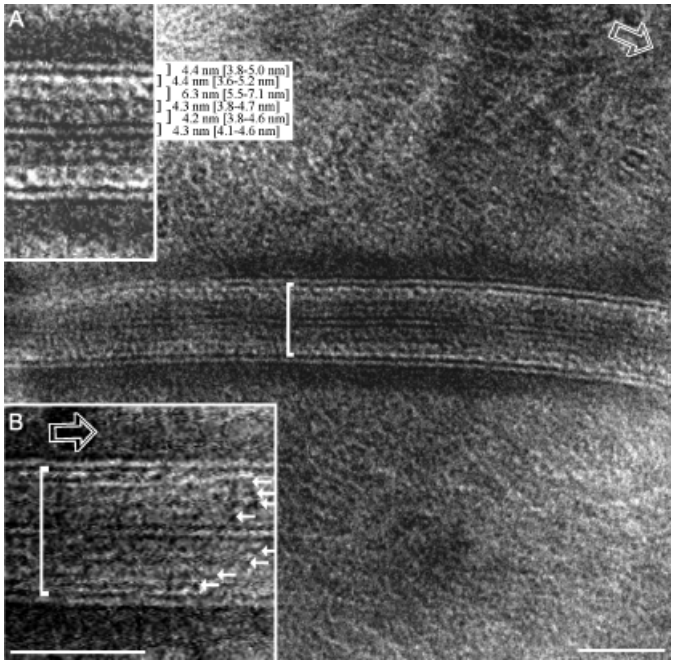

Figure 8
The ~ 44 nm thick regions (*A*) express a characteristic eight-line pattern between adjacent corneocyte lipid envelopes. High-magnification cryo-transmission electron micrographs of vitreous mid-part stratum corneum. The dominating ~ 44 nm thick regions express eight parallel electron-dense lines with different, but characteristic, intensity and spacing between adjacent corneocyte lipid envelopes (*inset box A*). *Inset box* (*A*): represents a magnification of the area marked by a square bracket. A relatively rare variant with a thickness of ~ 48 nm (*inset box B*, *white square bracket*) expresses a ten-line pattern (*inset box B*, *thin white arrows*) instead of the more common eight-line pattern (*inset box A*). *Open white double arrows*: section cutting direction. Section thickness ~ 50 nm. *Scale bars*: 50 nm.

The earlier reported multilamellar ~ 13 nm periodicity of the stratum corneum extracellular space, showing a broad–narrow–broad electron lucent band pattern (Madison *et al*, 1987; Swartzendruber *et al*, 1989; Hou *et al*, 1991), was not observed in this study. This discrepancy may be because of morphological changes induced by fixation and/or dehydration during conventional sample preparation for electron microscopy. But as the OD of conventional electron micrographs is directly related to the chemical ability to bind stain, whereas for cryo-electron micrographs of vitreous sections the OD is directly related to the local density of biomaterial in the section, a direct comparison is not straightforward.

SAXD on stratum corneum has shown 4.0–4.4, 5.8–6.6, and 12.9–13.6 nm reflections attributed to lipids (Bouwstra *et al*, 1991; Garson *et al*, 1991; Hou *et al*, 1991; Schreiner *et al*, 2000; Ohta *et al*, 2003) and 8.6–9.5, 12.5–14.5, and 25.0–27.0 nm reflections attributed to proteins (Swanbeck, 1959a, b; Bouwstra *et al*, 1991; Garson *et al*, 1991). The direct linking of these results to the cryo-electron density patterns observed in this study is difficult.

Conventional electron microscopy and immunocytochemistry studies have shown that non-peripheral desmosomes gradually are lost in the lower stratum corneum whereas corneodesmosomes on the corneocyte cell edges persist into the final desquamation (Lundström and Egelrud, 1988; Skerrow *et al*, 1989; Chapman and Walsh, 1990; Mils *et al*, 1992; Haftek *et al*, 1998). This study does not exclude this possibility. Further, one high-magnification micrograph obtained from the lower stratum corneum showed a desmosome-like structure with a well-developed cytoplasmic plaque and electron-dense plasma membrane (Fig 10*A*), which could correspond to a corneodesmosome structure. The apparent lack of the characteristic desmosome cadherin ~ 5 nm periodicity (cf. Fig 2) could, however, be because of an suboptimal orientation in the section and/or

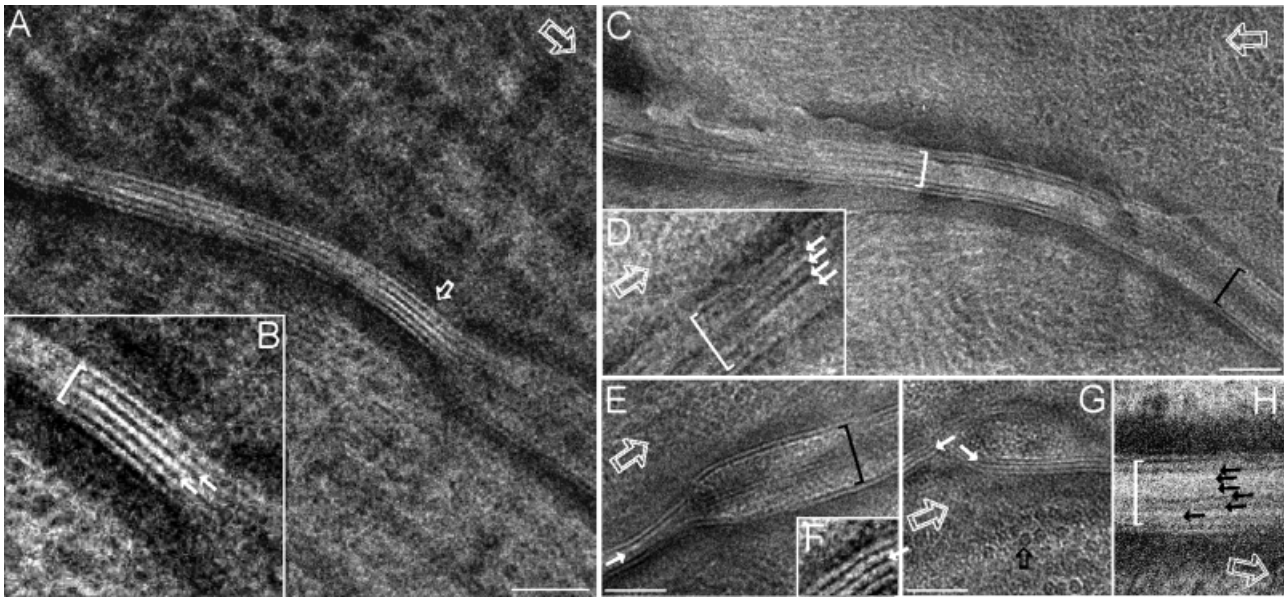

Figure 9
Linker-regions express one, two, four, and six parallel electron-dense lines, respectively. High-magnification cryo-transmission electron micrographs of vitreous mid-part stratum corneum (*A–H*). (*A*, *B*) ~ 14 nm thick (*B*, *white square bracket*) linker region containing two electron-dense lines (*B*, *thin white arrows*) between adjacent corneocyte lipid envelopes. (*B*) Represents a magnification of the area marked by an open white arrow in (*A*). (*C*, *D*) ~ 25 nm thick (*white brackets*) linker regions containing four lines (*D*, *thin white arrows*). (*C*) The four-line linker region is associated to an ~ 44 nm thick eight-line region (*C*, *black square bracket*). (*E–G*) ~ 9 nm thick linker regions containing one line (*thin white arrows*). Linker regions are particularly abundant in the cell periphery (*G*). (*E*) The one-line linker region (*thin white arrow*) is associated to an ~ 44 nm thick eight-line region (*E*, *black square bracket*). (*H*) ~ 33 nm thick (*whiter square bracket*) six-line (*thin black arrows*) linker region (cf. Fig 7*C*). *Open black arrow* (*G*): individual keratin intermediate filaments cut perpendicularly. *Open white double arrows* (*A–H*): section cutting direction. Section thicknesses (*A–H*) ~ 50 nm. *Scale bars*: (*A*, *C–E*, *G*), 50 nm.

suboptimal imaging conditions. Nonetheless, at medium magnification, very few regions, even at the cell periphery, seemed to express a characteristic cytoplasmic plaque electron density pattern (cf. Figs 1 and 5*B–D*). However, a variant of the ~ 44 nm thick regions, retaining a cytoplasmic plaque structure, does exist in the lower stratum corneum (Fig 10*B*, *solid black arrows*). Furthermore, the linker regions are both longer and more abundant at the corneocyte cell periphery (Fig 5*C*, *D*, *solid black arrows*), which supports the notion of a morphological difference between flat and peripheral corneocyte areas. Freeze-substitution electron microscopy (cf. Pfeiffer *et al*, 2000) combined with immunocytochemistry could perhaps give quantitative insights into these matters.

Transition state: The extracellular space between viable and cornified epidermis Roughly half of the length of the extracellular space at the interface between the stratum granulosum and stratum corneum of vitreous cryo-fixed epidermis was occupied by desmosomes at different stages of reorganization (Fig 1, *solid white arrows*) and the remaining half by widened areas (Fig 1, *thin white arrows*).

Widened areas The most frequently observed electron density patterns of inter-transition desmosomal widened areas of the extracellular space between viable and cornified epidermis were bent, stacked multilamellar (n = 19), and diffuse granular (n = 25) electron density patterns. Other characteristic structures were, however, also observed. Of these the most prevalent was an electron density check pattern (n = 5) marked by a white box in Fig 3*A*. The check pattern resembles, including its dimension, the cryo-electron microscopy density pattern of lipid/water *in vitro* phases with cubic symmetry (Fig 3*A*, *inset box*). A superposition of stacks of lamellae in the section thickness dimension could perhaps also account for this pattern.

A second pattern was a bent multilamellar electron density (Fig 3*B*) fully enclosing a granular electron density (*white box*) (n = 1). Fig 3*B* does not show a direct connection between the multilamellar complex and the extracellular space. It is, however, probably connected outside of the section plane (*solid white arrows in inset box*). Its pattern shows global similarities (with the exception of the scale) to cubic-to-lamellar membrane transitions observed in myeloid bodies of retinal pigment epithelium (Ahn, 1971; Landh, 1996, p. 81) and in the ER of UT-1 cells (Pathak *et al*, 1986) (*white box*). Further, similar electron density patterns have been reported in hamster cheek pouch stratum corneum (Hayward, 1978) and in porcine palatal stratum corneum (Swartzendruber *et al*, 1995), respectively. Also, widened areas of the interface between the stratum granulosum and stratum corneum of human epidermis have been reported to contain bent multilamellar lipid sheets associated with diffuse granular-like material (Fartasch *et al*, 1993).

The stacked, flattened multicircular electron density pattern of Fig 4*B* (*white box*) (n = 4) is remarkable by the complexity of the membrane-like structures and by the fact that, at several places, the line pattern seems to be closed on itself (*thin white arrow*). It is, however, evident that these apparently closed linear structures cannot represent flattened lipid vesicles (cf. "lamellar body discs"; Landmann,

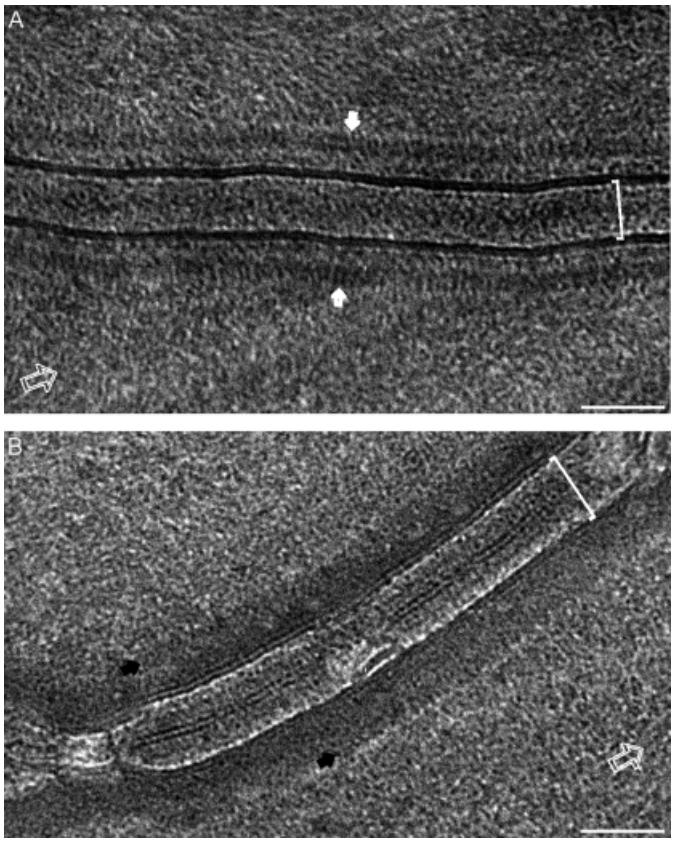

Figure 10
Corneodesmosomes? High-magnification cryo-transmission electron micrographs of vitreous lower mid-part stratum corneum (*A*, *B*). (*A*) Desmosome-like structure (cf. Fig 2) expressing a bilateral periodic cytoplasmic plaque pattern (*solid white arrows*). (*B*) $\sim$ 44 nm thick region-like structure expressing a cytoplasmic plaque (*solid black arrows*) on the cytoplasmic sides of the cornified envelopes. Structures expressing cytoplasmic plaques (*A*, *B*) are rare in the stratum corneum (cf. Figs 1 and 5*B–D*). *Open white double-arrows* (*A*, *B*): section cutting direction. Section thickness (*A*, *B*) $\sim$ 50 nm. *Scale bar*: (*A*, *B*), 50 nm.

1986) as their thickness (measured as the center-to-center distance between the two apposed electron-dense lines) is $<$4 nm, whereas a flattened lipid bilayer vesicle would be composed of two apposed $\sim$ 4 nm lipid bilayers yielding a total thickness of at least $\sim$ 8 nm. The complex electron density pattern observed may, however, be compatible with a single and coherent reversed bicontinuous lipid structure. Other interpretations, like e.g., that of a reversed oilcontinuous micellar lipid morphology (e.g., Q227-like, cf. Luzzati, 1997), are also possible.

In the first to third extracellular space of the stratum corneum, loosely packed extended lipid bilayer-like structures were observed in remaining widened areas (n = 14) (Fig 6*A*). Similar loosely arranged extended lamellae have been observed previously in conventional electron microscopy preparations (Menon *et al*, 1992; Fartasch *et al*, 1993). The loosely packed lipid bilayer-like structures were sometimes observed to be in possible continuity both with linker regions (Fig 7*A*, *C*) and with $\sim$ 44 nm and 39 nm thick eight-line regions (Fig 6*B*, *C*). No widened areas were observed above the third stratum corneum extracellular space. Close packing of stacked lipid bilayers of widened areas may thus be at the origin of both linker (one, two, four, six line) and thick (eight and ten lines) regions of the mature (i.e., above the third) stratum corneum extracellular space.

Transition desmosomes Epidermal desmosomes undergo a pronounced reorganization at the interface between the stratum granulosum and stratum corneum (Fig 1) involving: (a) a widening of the desmosome extracellular core domain from $\sim$ 33 to $\sim$ 43 nm (Table I); (b) the disappearance of the desmosome extracellular core domain transverse $\sim$5 nm periodicity; (c) the appearance of an eight-line electron density pattern of which a central double-layer pattern is the most electron dense (Fig 4*C*, *inset box*) and in which the line spacings are the same as in the $\sim$ 44 nm thick regions of the extracellular space of cornified epidermis (cf. Fig 8*A*); (d) the disappearance of the cytoplasmic plaque (Fig 3*A*, *solid black arrow*; Figs 4*A–D*, *solid white arrows*); (e) the appearance of the cornified envelope (Figs 4*A–D*, *solid black arrows*); and (f) a decrease in plasma-membrane electron density. Moreover, stacked lipid bilayer-like structures become closely associated laterally to the transition desmosome (Fig 4*D*, *region "1"*), sometimes apparently penetrating into the transition-desmosome extracellular core domain (Fig 4*A*, *open white arrow*), as judged from the local presence of a remaining desmosome cytoplasmic plaque (Fig 4*A*, *solid white arrow*). A close association between extradesmosomal lipid bilayer structures and transition desmosome "plugs" has also been observed by conventional electron microscopy (Fartasch *et al*, 1993).

Hypothetical synthetic model for the transformation of the extracellular space during epidermal differentiation Figure 11 schematizes the major states of the transformation. The transformation starts in the upper part of the viable epidermis (state 1) where the intercellular space is constituted by desmosomes and their interspace. No fine structure has yet been resolved in the latter.

A major change takes place in the extracellular space between viable and cornified epidermis (state 2, lower part). Here desmosomes become transition desmosomes, described in detail above, and the inter-desmosomal space becomes widened into a bag containing highly complex membrane-like material. Our results do not support the view that this material represents stacks of flattened lipid bilayer vesicles (cf. Landmann, 1986). In contrast, all observations made so far seem to fit with a membrane folding process (cf. Norlén, 2001).

The transformation continues in the first few layers of the cornified epidermis (state 2, upper part) and ends (state 3) with the formation of $\sim$ 44 nm thick eight-line regions, derived from transition desmosomes, interconnected by one-, two-, four-, six-line linker regions and eight-, ten-line regions, derived from lamellar closepacking in remaining widened areas of two, three, five, seven, nine, and eleven lipid bilayers, respectively.

It is noteworthy that the desmosome transformation process seems morphologically continuous. Viable desmosomes do not simply become replaced by $\sim$ 44 nm thick regions. Instead, transition desmosomes retain many resemblances with their parent desmosomes. Similarly, the final $\sim$ 44 nm thick regions are closely reminiscent of transition desmosomes. It is fair to say, however, that the close

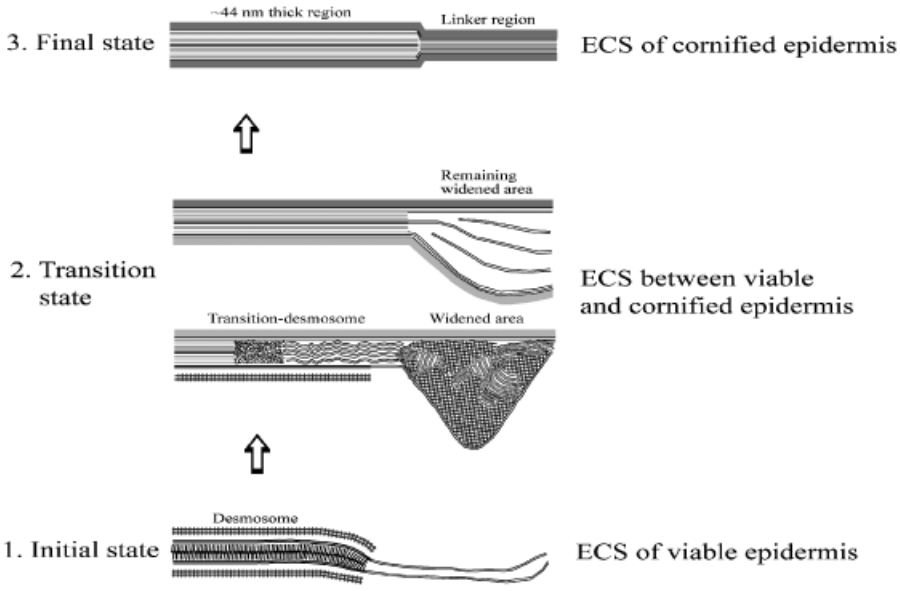

Figure 11
Hypothetical synthetic model for the transformation of the extracellular space (ECS) during epidermal differentiation. (1) Initial state: The upper part of the viable epidermis is constituted by desmosomes and their interspace. (2) Transition state: Desmosomes become transition desmosomes and the interdesmosomal space becomes widened into a bag containing highly complex membrane-like material. In the first few layers of the cornified epidermis remaining widened areas contain loosely packed extended lipid bilayers, which subsequently are closepacked into multilamellar sheets. (3) Final state: The mature corneocyte extracellular space is constituted by ~ 44 nm thick eight-line regions interconnected by linker regions. The ~ 44 nm thick regions may mainly be derived from transition desmosomes and possibly indirectly from widened areas. The linker regions may mainly be derived from widened areas.

relationship between desmosomes and ~ 44 nm thick regions is difficult to recognize without a detailed view of the complex nanostructure of transition desmosomes. Speculatively, the eight-line band pattern of the ~ 44 nm thick regions may be related to the recently proposed arrangement of cadherin ectodomains of the desmosome extracellular core domain (Garrod *et al*, 2002). The central double-layer pattern in Fig 8*A* and inset box in Fig 4*C* would then relate to the limit of desmosome EC1 ectodomains binding the cadherin molecules from both sides whereas the three bands on each side would relate to the limit between desmosome ectodomains EC2/3, EC3/4, and EC4/5, respectively. This observation could point to a new function of cadherin involving direct interactions between lipid and protein domains.

Materials and Methods

The study was approved by the authors' Institutional Review Board and was conducted according to the Declaration of Helsinki principles.

A total of >500 vitreous epidermal sections were examined. The study should be regarded as qualitative because of the fact that most structures described below are very small (a few nanometers) compared with the section thickness (~ 50 nm). Consequently, their visualization depends on their correct orientation in the section with respect to the viewing direction. Quantitative conclusions are therefore difficult to make and will have to wait until 3D reconstruction by computerized electron tomography has been developed.

In order to minimize the effect of section compression, all dimensions were exclusively measured approximately perpendicular to the cutting direction. Measures are given as medians of means together with range and number of observations (n) (n = number of independent biological structures with a given morphology observed with an instrumental resolution of <2 nm). The mean value of five measurements performed on each observation was used to calculate the median and range for each population of independent observations.

The thickness of the extracellular space was measured as the center-to-center distance between the outer electron-dense line of the double-layer patterns forming the keratinocyte plasmamembranes, or corneocyte lipid envelopes, of two apposed cells.

Throughout the manuscript, the term "double-layer pattern" refers to two parallel electron-dense lines and the term "lipid bilayer" refers to a biological structure largely composed of lipids in a bilayer conformation (either normal or reversed).

Tissue preparation Five skin biopsies were taken during the winter of 2002/2003 from the mid-portion of the left volar forearm of each of four healthy (as judged by dermatological examination) Caucasian male subjects (25–35 y old) who had no history of dermatological disease. All participants in the study had given their informed consent. The skin area used had not been exposed to any detergents, treatments, or skin care products for 1 month prior to experimentation. The biopsies were immediately submerged in 1-hexadecane to avoid dehydration during cutting. The samples were cut with a double-edged razorblade into 1×1 mm^2 large pieces with a thickness of approximately 100–150 μm.

Processing for cryo-transmission electron microscopy The 1×1 mm^2 samples were placed in the cavity (diameter 2 mm; depth 0.1 mm) of a cylindrical aluminum platelet (diameter 3 mm; thickness 0.5 mm) and covered by a second matching flat aluminum platelet. The cavity space not occupied by the sample was filled with 1-hexadecane (Fluka, Buchs, Switzerland).

The high-pressure freezer HPM 010 (Baltec, Balzers, Liechtenstein), which reaches a pressure of 2000 bar within 15 ms, was used. The high pressure was built up at a controlled temperature by the use of a defined volume of thermostatized ethanol that hit the sample before the pressurized liquid nitrogen and thus ensured a stable correlation between rise in pressure and drop in temperature (cf. Moor, 1987). The samples were cryo-fixed within 90 s after the biopsies were taken.

For a general description, and more technical details, of cryo-electron microscopy of vitreous specimens cf. Dubochet *et al* (1988) and Al-Amoudi *et al* (2004), and references therein. Small pieces of the high-pressure frozen epidermal forearm samples were glued to aluminum pins in an FCS cryo-chamber of an Ultracut S microtome (Leica, Vienna, Austria). The vitreous samples were trimmed with a trimming diamond knife (Diatome, Biel, Switzerland) and cryo-sectioned at -160°C with a nominal section thickness of 50 nm using a 45° diamond knife (Diatome) with a clearance angle of 6°. Cutting speed was set to 0.6 mm per s. The sections were transferred to carbon-film-covered 400 and 1500 mesh copper grids using an eyelash glued to a wooden stick. Subsequently the sections were pressed with a stamping tool and

stored in liquid nitrogen. A facemask was used throughout the section transfer procedure to minimize ice-crystal contamination. Air flow, temperature, and humidity were controlled in the working room.

The copper grids with the mechanically attached vitreous epidermal sections were transferred to a Gatan cryo-holder (Gatan, Warrendale, Pennsylvania) at -180°C and inserted into a Phillips CM12 cryo-electron microscope (Philips, Eindhoven, the Netherlands). The accelerating voltage was 80 kV, the objective aperture was 50 μm and, the camera length was 370 mm. The applied electron dose was always <1000 e per nm^2 per micrograph and the electronic magnification was in the 400–45,000 $\times$ range. Images were recorded digitally with the use of a Gatan CCD camera (Gatan) or on Kodak SO 165 photographic films (Kodak, Geneva, Switzerland). The microscope magnification was recalibrated prior to the first data collection to ensure an error of less than 2%.

Complete vitrification of the observed cryo-sections was checked by electron diffraction. Non-vitrified specimens were discarded.

Defocus and instrumental image resolution (as judged from the extension of Thon's rings) was calculated using the EMtool software (Ludtke, 1996).

The OD of micrographs to be compared were calibrated with a standard negative of known OD. Contrast between adjacent regions with different OD_1 and OD_2 was defined as $(OD_1-OD_2)/((OD_1+OD_2)/2)$. OD was measured using a transmission densitometer (Melico/Photolog, Medical & Electrical Instrumentation, London, UK).

The thickness of the sections was determined from their contrast on the micrographs, on the basis of the following relation (cf. Dubochet *et al*, 1983):

$$\rho t = \Lambda \ln(OD_h/OD_s)$$

where OD_s represents the OD of the different biological structures of the sample, OD_h represents the OD of a hole in the section, ρ is the density, t is the section thickness, and Λ is the mean free mass thickness that, for our working conditions, has a value of 200 mg per m^2 (cf. Dubochet *et al*, 1983).

This work was made possible by the generous support from the Wenner-Gren Foundations (L. N.), the Schmidheiny Foundation (L. N.), and the Welander Foundation (L. N.). We are indebted to Professor Pierre Descouts, GAP-Biomedical, University of Geneva, without whom this project would not have been possible. We would further like to thank Dr Tomas Landh, Professor Kåre Larsson, and Professor Vittorio Luzzati for innumerable discussions and unfailing interest. We also thank our reviewers for their many helpful comments and suggestions.

DOI: 10.1111/j.0022-202X.2005.23630.x

Manuscript received April 7, 2004; revised November 3, 2004; accepted for publication November 5, 2004

Address correspondence to: Lars Norlén, Medical Nobel Institute, Department of Cell and Molecular Biology (CMB), Nobels v. 3, Karolinska Institutet, 171 77 Stockholm, Sweden. Email: lars.norlen@physics.unige.ch

References

Ahn JNH: Les corps myéloïdes de l'épithelium pigmentaire rétinien. I. Répartition, morphologie et rapports avec les organites cellulaires. Z Zellforsch 115:508–523, 1971

Al-Amoudi A, Norlén LPO, Dubochet J: Cryo-electron microscopy of vitreous sections of native tissue. J Struct Biol 148:131–135, 2004

Blank IH: Factors which influence the water content of stratum corneum. J Invest Dermatol 18:433–440, 1952

Bouwstra JA, Dubbelaar FER, Gooris GS, Ponec M: The lipid organisation in the skin barrier. Acta Derm Venerol 208 (Suppl.):23–30, 2000

Bouwstra JA, Gooris GS, Van der Spek JA, Bras WW: Structural investigations of human stratum corneum by small-angle x-ray scattering. J Invest Dermatol 97:1005–1012, 1991

Burdett IDJ: Aspects of the structure and assembly of desmosomes. Micron 29:309–328, 1998

Chapman SJ, Walsh A: Desmosomes, corneosomes and desquamation. An ultrastructural study of adult pig epidermis. Arch Dermatol Res 282: 304–310, 1990

Dubochet J, Adrian M, Chang J-J, Homo J-C, Lepault J, McDowall AW, Schultz P: Cryo electron microscopy of vitrified specimens. Quart Rev Biophys 21:129–228, 1988

Dubochet J, McDowall AW, Menge B, Schmid EN, Lickfeld KG: Electron microscopy of frozen-hydrated bacteria. J Bacteriol 155:381–390, 1983

Evans FD, Wennerström H: The Colloidal Domain: Where Physics, Chemistry, Biology and Technology Meet. New York: VCH Publishers, 1994

Fartasch M, Bassukas ID, Diepgen T: Structural relationship between epidermal lipid lamellae, lamellar bodies and desmosomes in human epidermis: An ultrastructural study. Br J Dermatol 128:1–9, 1993

Garrod DR, Merritt AJ, Nie Z: Desmosomal cadherins. Curr Opin Cell Biol 14: 537–545, 2002

Garson J-C, Doucet J, Lévêque J-L, Tsoucaris G: Oriented structure in human stratum corneum revealed by x-ray diffraction. J Invest Dermatol 96: 43–49, 1991

Guldbrand L, Jönsson B, Wennerström H: Hydration forces and phase equilibria in the dipalmitoyl phosphatidylcholine-water system. J Colloid Interface Sci 89:532–541, 1982

Haftek M, Teillon M-H, Schmitt D: Stratum corneum, corneodesmosomes and *ex vivo* percutaneous penetration. Microsc Res Technol 43:242–249, 1998

Hayward AF: Ultrastructural changes in contents of membrane-coating granules after extrusion from epithelial cells of hamster cheek pouch. Cell Tissue Res 187:323–331, 1978

He W, Cowin P, Stokes DL: Untangling desmosomal knots with electron tomography. Science 302:109–113, 2003

Hill JR, Wertz PW: Molecular models of the intercellular lipid lamellae from epidermal stratum corneum. Biochim Biophys Acta 1616:121–126, 2003

Hou SYE, Mitra AK, White SH, Menon GK, Ghadially R, Elias PM: Membrane structures in normal and essential fatty acid-deficient stratum corneum: Characterization by ruthenium tetroxide staining and X-ray diffraction. J Invest Dermatol 96:215–223, 1991

Israelachvili JN: Intermolecular and Surface Forces, 2nd edn. San Diego: Academic Press, 1992

Landh T: Cubic cell membrane architectures—taking another look at membrane bound cell spaces. Thesis, Department of Food Technology, Lund University, Lund, Sweden, 1996.

Landmann L: Epidermal permeability barrier: Transformation of lamellar granule-discs into intercellular sheets by a membrane-fusion process, a freeze-fracture study. J Invest Dermatol 87:202–209, 1986

Larsson K: Lipids: Molecular Organisation, Physical Functions and Technical Applications. Dundee, Scotland: The Oily Press, 1994

Ludtke S: EMtool® freeware, http://ncmi.bioch.bcm.tmc.edu/~stevel/emtool/frame.html, 1996

Lundström A, Egelrud T: Cell shedding from human plantar skin *in vitro*: Evidence on its dependence on endogenous proteolysis. J Invest Dermatol 91: 340–343, 1988

Luzzati V: Biological significance of lipid polymorphism: The cubic phases. Curr Opin Struct Biol 7:661–668, 1997

Madison KC, Swartzendruber DC, Wertz PW, Downing DT: Presence of intact intercellular lamellae in the upper layers of the stratum corneum. J Invest Dermatol 88:714–718, 1987

McIntosh TJ: Organization of skin stratum corneum extracellular lamellae: Diffraction evidence for asymmetric distribution of cholesterol. Biophys J 85:1675–1681, 2003

Menon GK, Feingold KR, Elias P: Lamellar body secretory response to barrier disruption. J Invest Dermatol 98:279–289, 1992

Mils V, Vincent C, Croute F, Serre G: The expression of desmosomal and corneodesmosomal antigens shows specific variations during terminal differentiation of epidermis and hair follicle epithelia. J Histochem Cytochem 40:1329–1337, 1992

Moor H: Theory and practice of high pressure freezing. In: Steinbrecht RA, Zierold K (eds). Cryo-Techniques in Biological Electron Microscopy. Berlin: Springer, 1987; p 175–179

Norlén LPO: Skin barrier formation—the membrane folding model. J Invest Dermatol 117:823–829, 2001

Norlén LPO, Al-Amoudi A: Stratum corneum keratin structure, function and formation—the cubic rod-packing and membrane templating model. J Invest Dermatol 123:715–732, 2004

Norlén LPO, Al-Amoudi A, Dubochet J: A cryo-transmission electron microscopy study of skin barrier formation. J Invest Dermatol 120:555–560, 2003

North AJ, Bardsley WG, Hyam J, *et al*: Molecular map of the desmosomal plaque. J Cell Sci 112:4325–4336, 1999

Ohta N, Ban S, Tanaka H, Nakata S, Hatta I: Swelling of the intercellular lipid lamellar structure with short repeat in hairless mouse stratum corneum as studied by X-ray diffraction. Chem Phys Lipids 123:1–8, 2003

Pathak RK, Luskey KL, Anderson RGW: Biogenesis of the crystalloid endoplasmic reticulum in UT-1 cells: Evidence that the newly formed endoplasmatic reticulum emerges from the nuclear envelope. J Cell Biol 102:2158–2168, 1986

Pfeiffer S, Vielhaber G, Vietzke J-P, Wittern K-P, Hintze U, Wepf R: High-pressure freezing provides new information on human epidermis: Simultaneous protein antigen and lamellar lipid structure preservation. Study on human epidermis by cryoimmobilization. J Invest Dermatol 114:1030–1038, 2000

Schreiner V, Gooris GS, Pfeiffer S, *et al*: Barrier characteristics of different human skin types investigated with X-ray diffraction, lipid analysis, and electron microscopy imaging. J Invest Dermatol 114:654–660, 2000

Skerrow CJ, Clelland DG, Skerrow D: Change to desmosomal antigens and lecitin-binding sites during differentiation in normal human epidermis: A quantitative study. J Cell Sci 92:667–677, 1989

Small DM: The Physical Chemistry of Lipids. Handbook of Lipid Research. New York: Plenum Press, 1986

Spicer PT, Hayden KL, Lynch ML, Ofori-Boateng A, Burns JL: Novel process for producing cubic liquid crystalline nanoparticles (cubosomes). Langmuir 17:5748–5756, 2001

Swanbeck G: On the keratin fibrils of the skin. An X-ray small angle scattering study of the horny layer. J Ultrastruct Res 3:51–57, 1959a

Swanbeck G: Macromolecular organisation of epidermal keratin. Acta Derm Venereol (Stockh) 39 (Suppl. 43):1–37, 1959b

Swartzendruber DC, Manganaro A, Madison KC, Kremer M, Wertz PW, Squier CA: Organization of the intercellular spaces of porcine epidermal and palatal stratum corneum: A quantitative study employing ruthenium tetroxide. Cell Tissue Res 279:271–276, 1995

Swartzendruber DC, Wertz PW, Kitko DJ, Madison KC, Downing DT: Molecular models of the intercellular lipid lamellae in mammalian stratum corneum. J Invest Dermatol 92:251–257, 1989